# In-place correction of diffraction distortion in Low-Energy Electron Microscopy

THESIS

submitted in partial fulfillment of the
requirements for the degree of

BACHELOR OF SCIENCE
in
PHYSICS AND MATHEMATICS


| | |
|---|---|
| Author : | Lionel Kielhöfer |
| Student ID : | s1978462 |
| Supervisor : | T.A de Jong, MSc |
| | Prof.dr.ir. S.J. van der Molen |
| $2^{nd}$ corrector : | D.N.L Kok, MSc |
| | Prof.dr. K.J. Batenburg |


Leiden, The Netherlands, August 12, 2022

# In-place correction of diffraction distortion in Low-Energy Electron Microscopy

**Lionel Kielhöfer**

Huygens-Kamerlingh Onnes Laboratory, Leiden University
P.O. Box 9500, 2300 RA Leiden, The Netherlands

August 12, 2022

## Abstract

Diffraction distortion in LEEM diffraction imaging makes it impossible to measure angles and distances accurately. In a LEEM this diffraction distortion changes when the sample measured is changed meaning it needs to be corrected each time. In this thesis the method for an in-place correction is explained and applied. The method successfully allows the measurement of angles and distances without requiring the measurement of too much data. However, it can still be improved upon so that less data is needed and a better correction is acquired.

# Contents

Chapter 1

# Introduction

To find out about the atomic lattice structure of a sample one would like to image it. This way one can measure distances and angles in the lattice structure. This is done using electron diffraction. In electron diffraction electrons are accelerated towards the sample and then scatter creating a diffraction image. The diffraction image images the reciprocal lattice instead of the atomic lattice. However, the reciprocal lattice can be used to find the atomic lattice as they are directly related.

Electron diffraction is done in a Low-Energy Electron Microscope (LEEM). A LEEM is not only used for electron diffraction, it can also make real space images. The real space images it can make are, however, several scales larger than required for imaging an atomic lattice. A LEEM is a big machine with a lot of components that interact with the electrons. Because of this there is often a strong distortion in the resulting diffraction images. This is problematic as it prevents the measuring of angles and distances in the diffraction images and therefore the atomic lattice.

To correct this distortion in a dedicated Low-Energy Electron Diffraction (LEED) machine one would measure a known sample to calibrate the machine. This is done in [1]. However, in a LEEM setup this is not possible. Replacing a sample causes the LEEM setup to be decalibrated. Therefore, an in-place correction of the diffraction distortion needs to be done. That is, a correction of the diffraction distortion that can be performed without replacing the sample even for samples with an unknown diffraction pattern or lattice structure.

The method in this thesis uses the deflectors present in a LEEM setup to move the sample in k-space. This movement in k-space can be controlled. However, due to the distortion the resulting diffraction image will have moved differently in k-space. Doing this an in-place calibration image

can be formed for which the undistorted image is known. From this the distortion function is found and then removed from the images.

Chapter 2

# Background

To find the atomic lattice structure of a material one can try to image its lattice directly. However, there exist only a few techniques that can accomplish a sufficiently high resolution to achieve this (e.g. scanning tunneling microscopy). This is because the scale at which the atomic lattice structure can be seen is so small. Neighbouring lattice points are usually only a couple of angstroms apart. By using LEEM diffraction imaging this problem can be circumvented. Instead of imaging the atomic lattice the reciprocal lattice is imaged. This is beneficial as the reciprocal lattice has a direct connection to its atomic lattice. In the next sections it is explained how the diffraction imaging in the LEEM works and how the resulting reciprocal lattice is related to its atomic lattice.

## 2.1 Reciprocal Lattice

This thesis aims to correct the distortion present in imaging a reciprocal lattice by a LEEM. Therefore it is useful to explain the mathematical meaning of a reciprocal lattice and the connection to its atomic lattice.

The samples imaged in a LEEM have 2-dimensional Bravais lattice structures. In general, a 2-dimensional Bravais lattice is the infinite set of discrete points given by:

$$\mathbf{R} = \{n_1\mathbf{a}_1 + n_2\mathbf{a}_2 : n_1, n_2 \in \mathbb{Z}\} \tag{2.1}$$

Here $\mathbf{a}_1, \mathbf{a}_2 \in \mathbb{R}^2$ are called the primitive vectors. If $\mathbf{R}$ is an atomic lattice then points in $\mathbf{R}$ are referred to as lattice points. The reciprocal lattice of $\mathbf{R}$ is then given by:

$$\mathbf{G} = \{\mathbf{k} : \forall \mathbf{r} \in \mathbf{R} : e^{i\mathbf{k}\cdot\mathbf{r}} = 1\} \tag{2.2}$$

If **R** is an atomic lattice, points in **G** are referred to as Bragg peaks. **G** will also be a Bravais lattice with primitive vectors given by:

$$\begin{aligned} \mathbf{b}_1 &= 2\pi \frac{B\mathbf{a}_2}{\mathbf{a}_1 \cdot B\mathbf{a}_2} \\ \mathbf{b}_2 &= 2\pi \frac{B\mathbf{a}_1}{\mathbf{a}_2 \cdot B\mathbf{a}_1} \end{aligned} \tag{2.3}$$

Where $B = \begin{pmatrix} 0 & -1 \\ 1 & 0 \end{pmatrix}$. One can represent the lattice **R** as the following sum of delta functions $f(\mathbf{x}) = \sum_{\mathbf{r}\in\mathbf{R}} \delta(\mathbf{x}-\mathbf{r}) = \sum_{n_1,n_2=-\infty}^{\infty} \delta(\mathbf{x} - n_1\mathbf{a}_1 - n_2\mathbf{a}_2)$. It can be shown that the Fourier transform of $f$, call it $g$, is a sum of delta functions such that $g(\mathbf{y}) = \sum_{\mathbf{k}\in\mathbf{G}} \delta(\mathbf{y}-\mathbf{k})$. It can also be shown that the reciprocal lattice of the reciprocal lattice of **R** is the lattice **R** [2, Chapter 13]. Thus once the reciprocal lattice of **R** is imaged, the lattice **R** is easily obtained by applying a Fourier transform.

## 2.2 LEEM Diffraction Imaging

Diffraction imaging is done by irradiating a sample with particles, in this case electrons, from a constant incident angle. As particles also exhibit wave properties they will interfere causing destructive and constructive interference. The scattered particles from the sample are then imaged, how this is done precisely is explained below. In this section the details on how a diffraction image is formed in a LEEM setup is discussed and how the distortion is caused in the process of imaging. But firstly, a brief reminder on how diffraction imaging can image the reciprocal lattice.

The condition for constructive interference between two particles in a lattice is given by the Bragg condition. This condition is equivalent to the Laue condition, which states that for a particle scattering from a wavevector of **k** to a wavevector of **k'** the difference $\mathbf{k} - \mathbf{k'}$ needs to be a reciprocal lattice vector [2, Chapter 14]. Thus the constructive interference images the reciprocal lattice.

A diffraction image is formed by focusing all the waves scattered at the same angle to the same spot on the detector. This can be seen in figure 2.1. As illustrated in figure 2.2, in a LEEM an image is formed as follows:

The electrons are released from the electron gun. The deflectors right under it can then be used to change the angle of incidence and position of the electrons onto the sample. Prism 1 then deflects the electrons onto the sample. The electrons then interact with the sample. $eV_0$ is the energy at which the electron arrive at the sample. This is called the landing energy. $eV_0$ can be adjusted to decide the energy at which the electrons interact with the sample. The scattered electrons from the sample

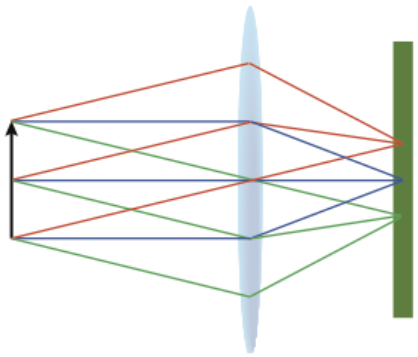

***Figure 2.1:*** *Copied from [3]. The arrow represents the sample. Each colour line represents a group of electrons scattering of the sample at the same angle. The lens in the middle then focuses each group to its own respective point on the detector on the right.*

are then re-accelerated back into the prism by the electrical field. Prism 1 then sends the electrons to Prism 2 which sends them to an electron mirror for aberration correction. After that Prism 2 sends the electrons to the detector. Along the way the electrons go through an aperture and the projector lenses. The aperture is used to remove secondary electrons caused by inelastic scattering and secondary electron generation effects. The lenses form the projector which amplify the image size to achieve magnification of the image. By turning certain lenses in the projector on or off one can switch between real space and diffraction images.

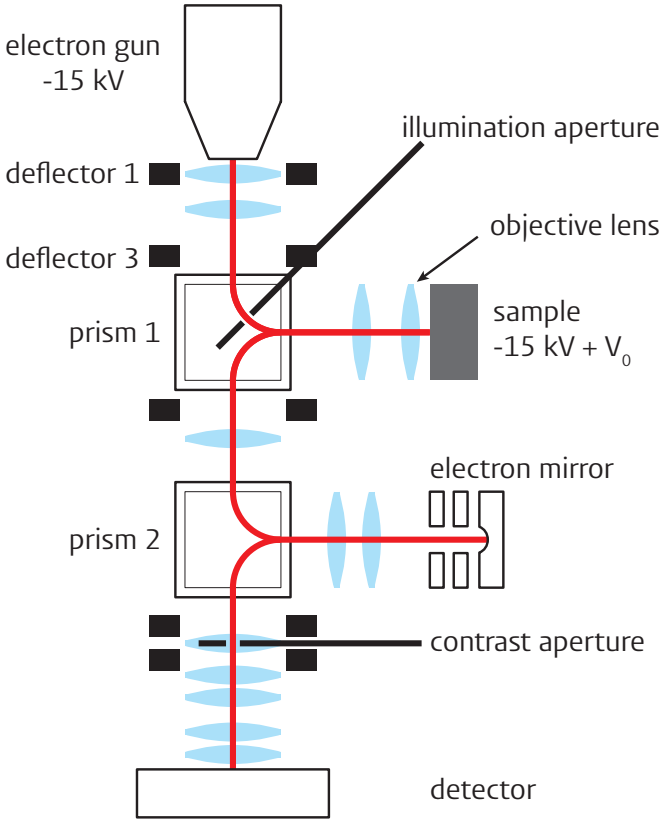


***Figure 2.2:*** *A schematic of the ESCHER LEEM in Leiden. Apertures and deflectors control the direction and number of electrons. $V_0$ controls the landing energy of the electrons. The second prism sends the electrons to an electron mirror for aberration correction. Lastly, the electrons are sent to the detector. This schematic was made by Johannes Jobst.*

Chapter 3

# Methods

Figure 3.1 is an example of a LEEM diffraction image. It is clear from this that there is a diffraction distortion. This diffraction distortion is caused by the electrons traveling through the setup. Instead of trying to correct this distortion by changing the setup one can correct the images without any changes to the setup necessary. The goal is to have a distorted LEED image of which the undistorted image is known. One can refer to the appendix for an overview of the symbols used throughout the method.

To do the in-place correction of the diffraction distortion the following will be done. Firstly, the transformation function for the diffraction distortion will be closely approximated. Then, the inverse transformation will be applied to LEED images. Finding the transformation function consists of a couple of steps explained in more detail below. The main idea is to generate a calibration image of which its corrected and diffraction distorted image is known. Using this the full transformation function can then be derived using interpolation.

## 3.1 Mathematical Setup

The images used are grayscale. Thus the following definition of an image will be used:

**Definition 1.** An image is a function $F$ from a finite discrete set $P \subset \mathbb{R}^2$ to $\mathbb{R}$. A point $x \in P$ is called a pixel, and $F(x)$ is called the intensity of that pixel. $P$ is called a pixel set.

For section 3.3 the center of a pixel set will be used. This is defined as follows:

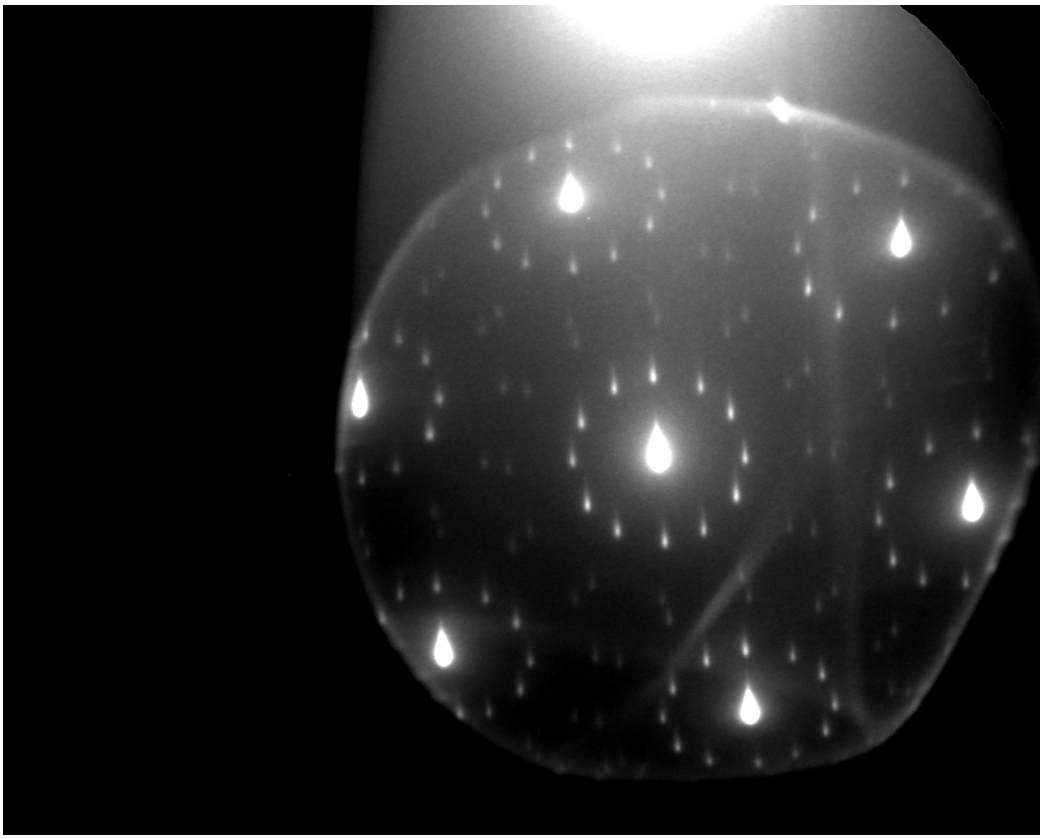

***Figure 3.1:*** *A diffraction image of the Charge Density Waves diffraction pattern in $TaS_2$ made with the ESCHER LEEM setup. The 12 spots around the 7 primary spots are meant to form a circle. However, this seems to only be the case for the central spot.*

**Definition 2.** Given a pixel set $P$ the average of the positions of all the pixels in $P$ is called the center of $P$.

Usually a pixel set is a regular grid, this is defined as follows:

**Definition 3.** A regular grid $G$ is a discrete subset of $\mathbb{R}^2$ that is defined by 2 perpendicular vectors, say $\mathbf{c}_1$ and $\mathbf{c}_2 \in \mathbb{R}^2$, two intervals, say $m$ and $n \in \mathbb{N}_0$ and a point $\mathbf{p} \in \mathbb{R}^2$ as follows:

$$G = \{\mathbf{p} + i\mathbf{c}_1 + j\mathbf{c}_2 : i \in \{0, ..., m\} \text{ and } j \in \{0, ..., n\}\} \tag{3.1}$$

A whole data set of images is defined as follows:

**Definition 4.** A data set of size $n \in \mathbb{N}_0$ is a set containing $n$ images.

Take an arbitrary LEED image $I$ with pixel set $P'$. Due to the diffraction distortion the pixel set $P'$ contains the distorted positions of the pixels. Therefore the image $I$ maps the intensities to the distorted pixel positions. Say that $P$ is the pixel set that contains the pixel positions without a distortion. Mathematically the diffraction distortion can then be seen as a function $T : \mathbb{R}^2 \to \mathbb{R}^2$ which maps $P$ to $P'$. From the setup it is expected for this function to be smooth. It is also expected for it to have certain other properties, these are discussed in section 3.3. The goal is thus to find this function $T$ as it allows one to map the right pixels to their intensities by the composite function $I \circ T$. This way the corrected image, denoted by $I_c$ can be written as:

$$I_c = I \circ T \tag{3.2}$$

Later on the term affine transformation will be used. An affine transformation is a composition of a translation and a linear map. An affine transformation $S : Q \mapsto U$ can be represented as follows:

$$S(x) = Dx + u \tag{3.3}$$

Where $D \in L(Q, U)$ * is a matrix and $u \in U$. This is used to represent the linear relationships between certain pixel sets after translating them.

## 3.2 Calibration Set

To be able to approximate the diffraction distortion a set $B'$ is needed of which the image $T^{-1}(B')$ is known. This set $B'$ will be called the calibration set. Take a LEED image $I : B' \to \mathbb{R}$. It is known that $B' = T(B)$ for a

*$D$ is in the set of all linear maps from $Q$ to $U$



Version of August 12, 2022– Created August 12, 2022 - 09:51

pixel set $B$ such that $I_c = I \circ T : B \to \mathbb{R}$ is the corrected image. In other words, a pixel set of which the correct and their respective distorted pixels are known has to be found.

Shifting the angle of incidence of the electron beam in a LEEM will result in another area of the reciprocal lattice to be imaged due to the electrons coming into the sample from a different angle. This effectively allows for the movement of the sample in k-space in a specified direction by shifting the angle of incidence appropriately. In a LEEM the electron beam deflectors are controlled by their own respective current. Changing the current in the $x$ or $y$ deflector in turn changes the incidence angle in their respective axis. This change is proportional to the effective movement of the sample in k-space [4]. In other words, when given values for the deflectors as in figure 3.2 a specific Bragg peak would move in k-space such that a regular grid is formed. Thus, a data set can be formed of LEED images at the deflector values in figure 3.2. This will be the data set referred to for the entire method. Then from this data set a specific Bragg peak is chosen. The position of this Bragg peak in each image then forms a pixel set, which will be denoted by $B'$, of which the points in the corresponding pixel set $B$, such that $B' = T(B)$, form a regular grid.

One can look at Figure 3.2 as a pixel set that is connected to $B$ by an affine transformation. This affine transformation connects the parameter space of the deflector to the position space in the sample. One can thus, after finding this transformation, construct the pixel set $B$. Thus generating the calibration set. To make this more formal, the pixel set from Figure 3.2 will be denoted as $C$. The transformation is defined as an affine transformation $L : \mathbb{R}^2 \to \mathbb{R}^2$ such that $L(C) = \{L(c) : c \in C\} = B$. For a $c \in C$, $L(c)$ would then be the actual position of the Bragg peak in k-space for the deflector values at $c$.

## 3.3 Affine Transformation

The goal of this section is to find the affine transformation $L$ from the previous section. As the set $B$ is not known this has to be done with another set which is known. It is known that for the set $B'$ the diffraction distortion is very weak in the center of each image, thus making $B'$ a good approximation of $B$ in the center. The reason for this is explained below. However, finding $B'$ is not directly possible thus another pixel set which can be found is taken. This pixel set, referred to as $M$, contains the pixels situated at the center of $B'$. At the end of this section it will be explained how this is used to find the affine transformation.

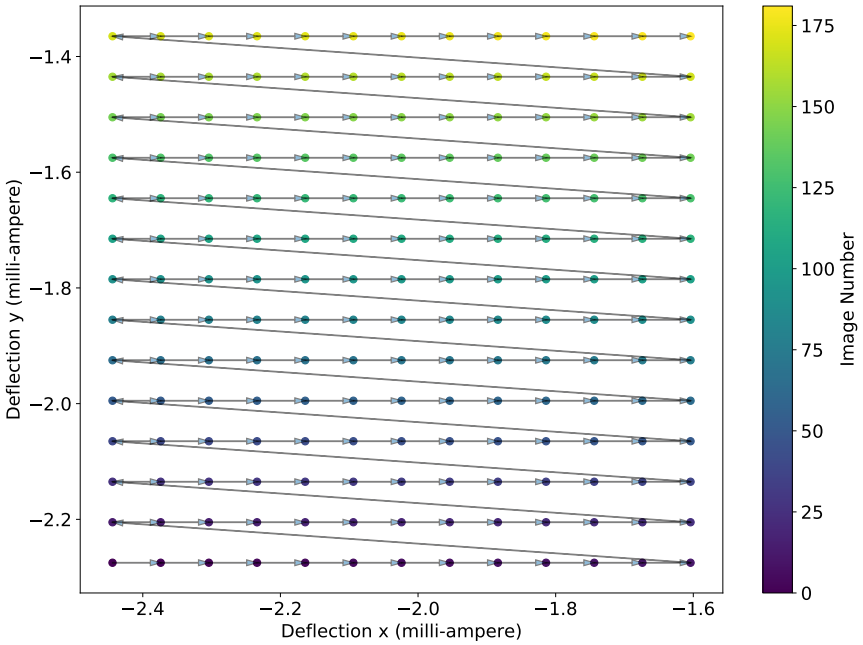


***Figure 3.2:*** *The value of the deflection for the angle of incidence (y over x) in milli-ampere. The colour gradient and the arrows show a scan order. This is the pixel set C.*



Version of August 12, 2022– Created August 12, 2022 - 09:51

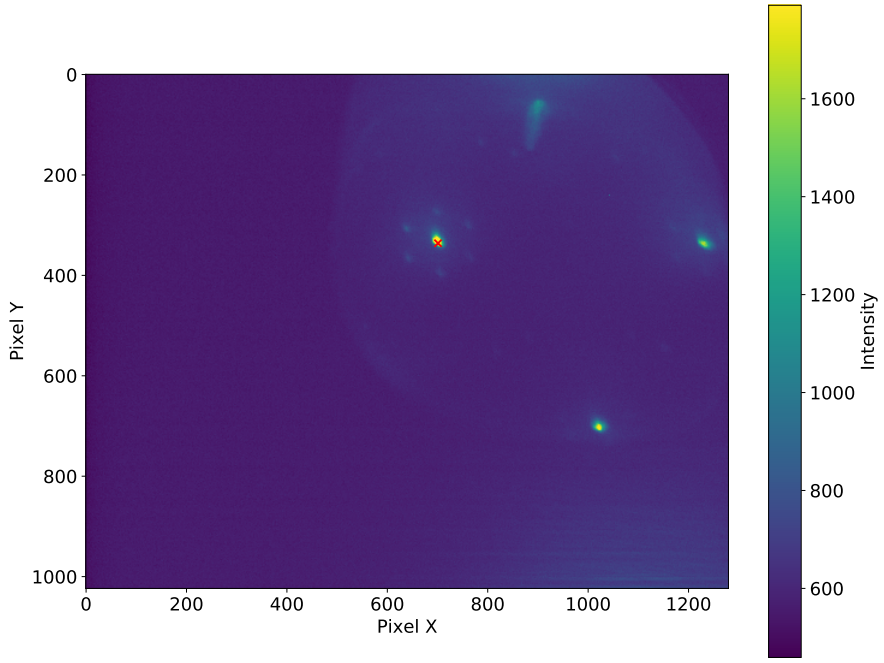


***Figure 3.3:*** *A LEED image of graphene on silicon carbide. The red cross represents the pixel with the highest intensity.*

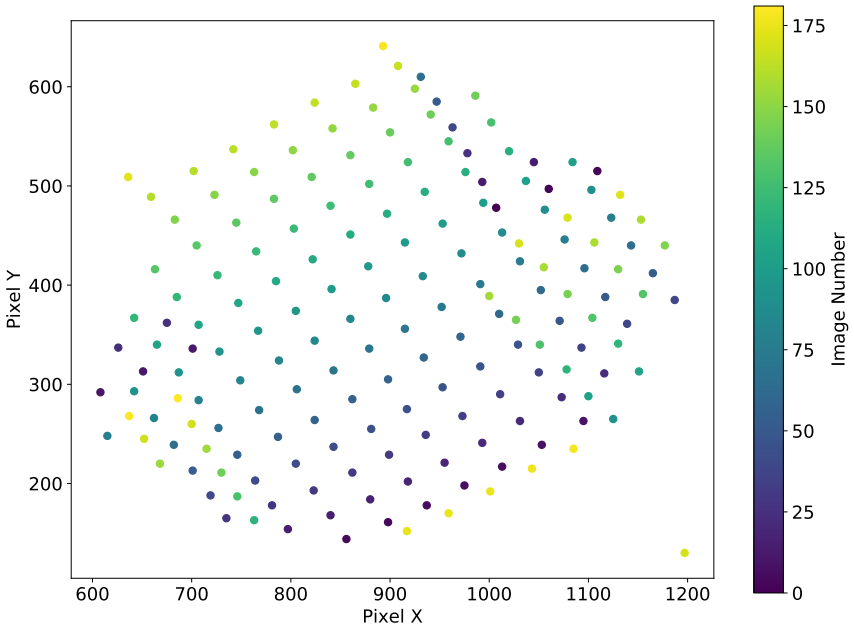


***Figure 3.4:*** *Pixel positions of the peaks with the maximum intensity in each image. The colour gradient corresponds to the scan order in Figure 3.2. This is the pixel set M.*

Say $T$ is written out as a Taylor expansion. The zeroth order coefficient can be set to 0 and the first order coefficient can be set as the identity matrix for the goal of this project. This is because these do not affect the distances and angles between Bragg peaks, and thus can be set to the given values for simplification. Furthermore, in the ESCHER LEEM setup at Leiden University there is a physical calibration in the setup that removes any second order distortion [4].This means that the diffraction distortion $T$ has very little effect in the center of $B$. In other words, $B'$ is a good first estimate of the pixel set $B$, especially in its center.

The set $M$ is found by taking the pixel with the highest intensity for each image in the data set. This is illustrated in figure 3.3. It can be seen in figure 3.4 that $M \neq B'$. This comes from the fact that the peak with the maximum intensity does not always represent the same Bragg peak. However, in the center of $M$ the pixels behave in the way that was expected of the pixel set $B'$. Thus the center pixels of $M$ are the same as that of $B'$. It is therefore possible to pick the center of $M$ such that no pixels represent other Bragg peaks. A problem that occurs is that the center of $M$ does not correspond to the center of $B'$. Instead a subset from the center of $C$ can be taken and the corresponding subset of $M$ can then be used due to this corresponding to a center subset of $B$ after applying $L$. This is illustrated in figure 3.5 and figure 3.6, these subsets will be referred to as $C_{sub}$ and $B'_{sub}$ respectively. More details about these subset are explained below.

As $L$ is an affine transformation it can be represented as:

$$L(x) = Ax + b \tag{3.4}$$

Where $A$ is a 2-by-2 matrix and $b \in \mathbb{R}^2$. The linear mapping happens around the centers of $C$ and $B$. In other words, given that $c_1$ is the center of $C$ and $c_2$ that of $B$:

$$A(x - c_1) + c_2 = L(x) \tag{3.5}$$

The center of $C$ is obtained by taking the component-wise mean of all its pixels. To obtain the center of $B$ the pixel set $B'_{sub}$ has to be used as $B$ is not known directly. The respective pixel set $C_{sub}$ then has to have a component-wise mean close to $c_1$ such that the component-wise mean can be used for $B'_{sub}$. This is done in Figure 3.5 by choosing a circle with a specific radius around $c_1$. From equations 3.4 and 3.5 it is now clear that $b = c_2 - Ac_1$.

The pixels in the pixel set $C, B, B'$ and $M$ can be ordered by their scan order. Because, as seen from before, each point in $C$ represents another image from which a point from $B, B'$ and $M$ is generated. The image index will be denoted by a subscript such that $C = \{x_1, ..., x_n\}$ with $n$ the total

images in the data set. In the same way $B, B'$ and $M$ will be reformulated. From this it follows that:

$$\forall x_i \in C : L(x_i) = Ax_i + b = y_i \in B \tag{3.6}$$

As $B$ is not known, a least squares minimization will be used with the set $B'_{sub}$ to find $L$ because, as stated before, the diffraction distortion should be very small on this pixel set. The minimization need only be used to find the remaining unknown $A$. This is done by finding an $A$ that minimizes the following sum:

$$\sum_{x_i \in C_{sub}} (Ax_i + b - y_i)^2 : y_i \in B'_{sub} \tag{3.7}$$

Finding this $A$ can be done using the Scipy function minimize.

## 3.4 Spline interpolation and Map Coordinates

Now that the affine transformation $L$ is known it can be applied to the pixels in $C$ to find $B$. Next only $B'$ is needed to determine $T$. Using $B'_{sub}$ restricts the amount of data that can be used for finding $T$. Also, $B'_{sub}$ was picked for its similarity to the appropriate subset of $B$, thus it shows little information about the diffraction distortion $T$. As stated before, pixels in $B$ should be close to their corresponding pixels in $B'$. Thus, in each image, one can look for the nearest peak to the corresponding pixel in $B$. This results in figure 3.7. From this it is clear that there is a diffraction distortion that gradually increases in strength as one gets further away from the center.

Both sets $B$ and $B'$ are pixel sets, thus they are discrete. This means that interpolation has to be used to find a close approximation of the diffraction distortion $T$. For this spline interpolation will be used, thus this approximation of $T$ will be denoted as $T_s$.

The pixels in the set $B$ will be denoted by $\mathbf{x}_i$ such that $B = \{\mathbf{x}_1, ..., \mathbf{x}_n\}$ and likewise for $B'$ as before. However, the $x$ and $y$ values of the pixels in the set $B'$ will be split such that a pixel $\mathbf{y}_i \in B'$ is represented as $\mathbf{y}_i = (a_i, b_i)$ with $a_i, b_i \in \mathbb{R}$. The diffraction distortion is also split into its $x$ and $y$ components represented as $T_x$ and $T_y$ respectively such that $T(\mathbf{x}) = (T_x(\mathbf{x}), T_y(\mathbf{x}))$ for arbitrary $\mathbf{x} \in \mathbb{R}^2$. This way $T_x, T_y : \mathbb{R}^2 \to \mathbb{R}$. In the same fashion $T_{s,x}$ and $T_{s,y}$ are defined.

Now the Scipy function SmoothBivariateSpline is used to find $T_{s,x}$ and $T_{s,y}$. The function does this by trying to fit a polynomial between each



Version of August 12, 2022– Created August 12, 2022 - 09:51

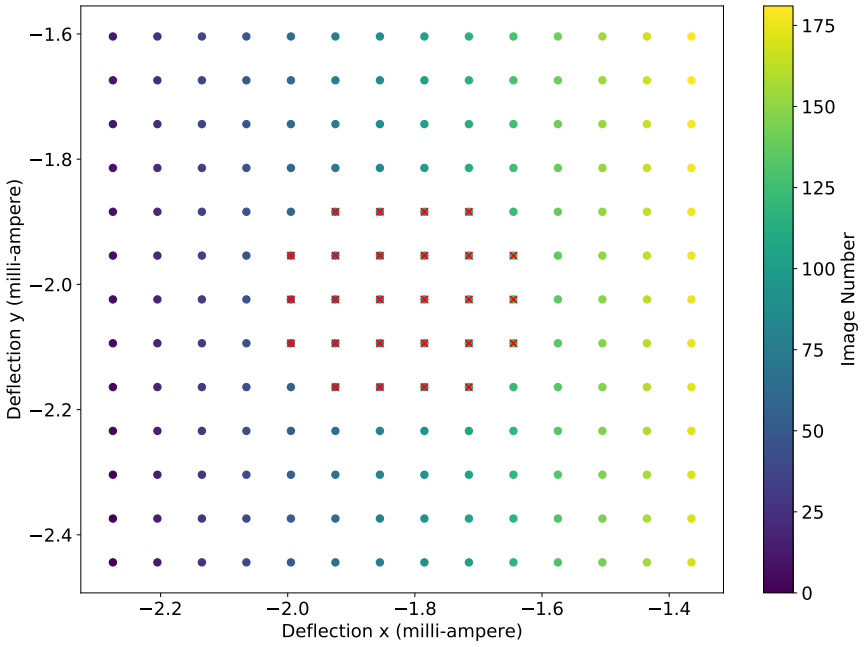


***Figure 3.5:*** *Figure 3.2 with red crosses representing the subset used for approximating the affine transformation. For the subset every data point within a ball of radius 0.2 milli-ampere around the mean was taken. This subset is the pixel set* $C_{sub}$.

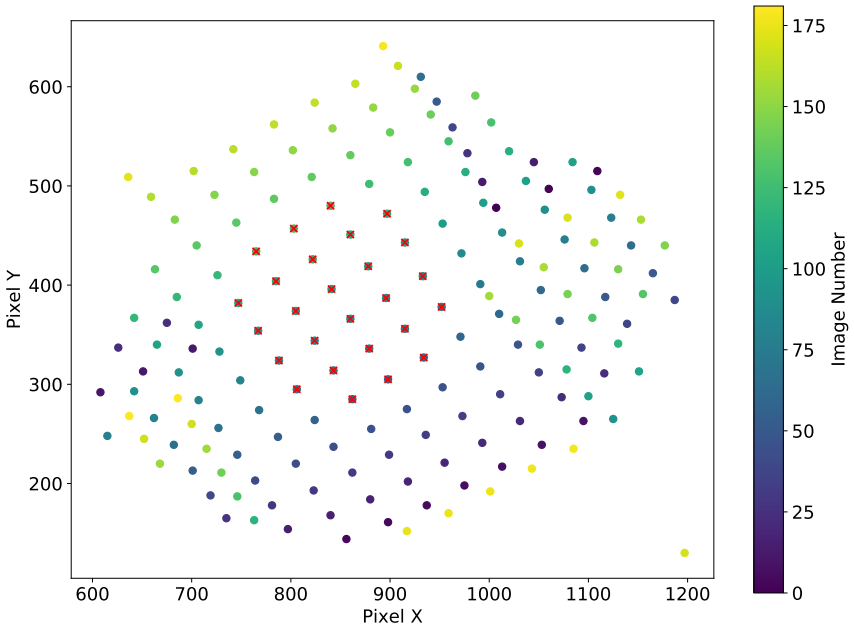


***Figure 3.6:*** *Figure 3.4 with red crosses representing the subset used for approximating the affine transformation. This subset corresponds to the one in Figure 3.5 by their scan order. This subset is the pixel set* $B'_{sub}$.

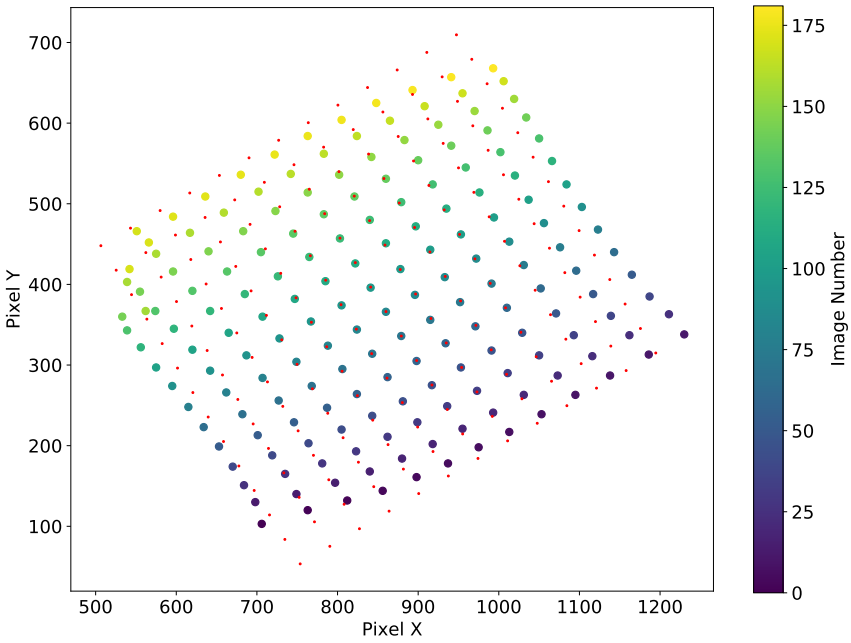


***Figure 3.7:*** *The red dots represent $B$ and the other coloured dots represent $B'$. For $B'$ the nearest peak to the location of where the lattice point should be, which is given by $B$, is taken. The peak with the highest intensity in a square of length 100 pixels centered around the lattice position was taken as the nearest peak. The colour gradient corresponds to the scan order in Figure 3.2.*

interval $(\mathbf{x}_i, \mathbf{x}_{i+1})$ for $i \in \{1, ..., n-1\}$. It does so in a way that the resulting function is smooth. This means that $T_{s,x}$ and $T_{s,y}$ are continuous and continuous in at least their first order derivatives [5] [6, Chapter 19.2].

The last step to correct the image is to map the corrected positions to their intensities as seen in equation 3.2. The problem with this is that most likely the corrected pixel set will not be a regular grid. For this reason interpolation has to be used again such that the domain of the corrected image is a regular grid. This is again done by spline interpolation through the Scipy function Map coordinates. This function takes the uncorrected image applied to the incorrect positions as input and also takes the correct positions as coordinates. It outputs the corrected image applied to a grid. It does this as follows. Using the coordinates given it determines for each point in the output the corresponding coordinate in the input. This is an approximate inverse of the diffraction distortion $T$. Then, the value of the input at those coordinates is determined by spline interpolation using the coordinates at which the input is already known.

Chapter 4

# Results

The goal of this chapter is to find out how much better the correction is to the original and in what ways fewer data points can be measured to get the best possible correction. The project is about making an in-place correction of the data. As a result of measuring less data, the calibrations would become a lot faster and therefore more useful. For this one must define a metric for the quality of the correction so that multiple different ways of taking less data can be compared. In this chapter, after introducing the metrics, we will use them to evaluate the performance of the correction on different subsets of the data. This will be used to find the best trade-off between quality and number of data points.

## 4.1 Metrics

Take a 2-dimensional reciprocal lattice like the one shown in figure 4.1. Take a scan area, which represents an image, as shown by the red box in figure 4.1. The difference vectors between all Bragg peaks inside the scan area are the same no matter where the scan area is on the lattice. Therefore, plotting these differences will result in a specific shape. For the graphene data used in this thesis, this shape is a perfect hexagon due to the sixfold symmetry of graphene *. The metrics introduced will measure different parts for the deviation of the observed data from a perfect hexagon. These therefore classify the quality of the distortion correction, which is the main source of deviation.

Firstly, the measured difference vectors will form clusters as seen in figure 4.2 and not 6 sharp positions of vertices like a perfect hexagon should.

*As the moire spots of graphene on silicon carbide are not taken into account here.

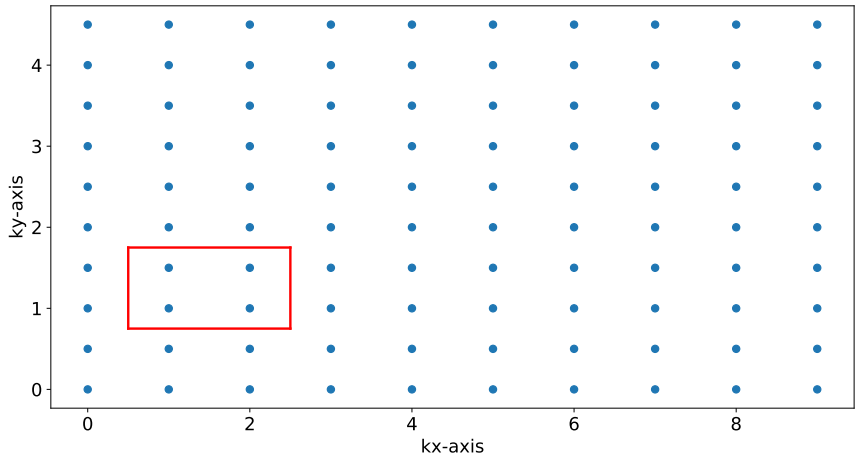


***Figure 4.1:*** *A reciprocal lattice with lattice constants* $(1, 0)$ *and* $(0, \frac{1}{2})$ *relative to the dimensions of the the axes. The red box is an example of a scan area.*

Therefore, the variance in these clusters defines a metric. This metric is used to find out the variance of angles and distances that should be the same. For the second metric, we note that the average can be taken in each of these clusters to form 6 sharp vertices of a deformed hexagon. The distance from the center of a perfect hexagon to a vertex is constant. Therefore, this variance in the deformed hexagon will be used as the second metric. Lastly, in a perfect hexagon, the angle between two vertices modulo 60 is 0 with the center of the perfect hexagon as reference point. The variance in these angles modulo 60 for the deformed hexagon is used for the third metric. The second and third metrics show how well the average distance or angle measured coincides with the actual distance or angle of the reciprocal lattice.

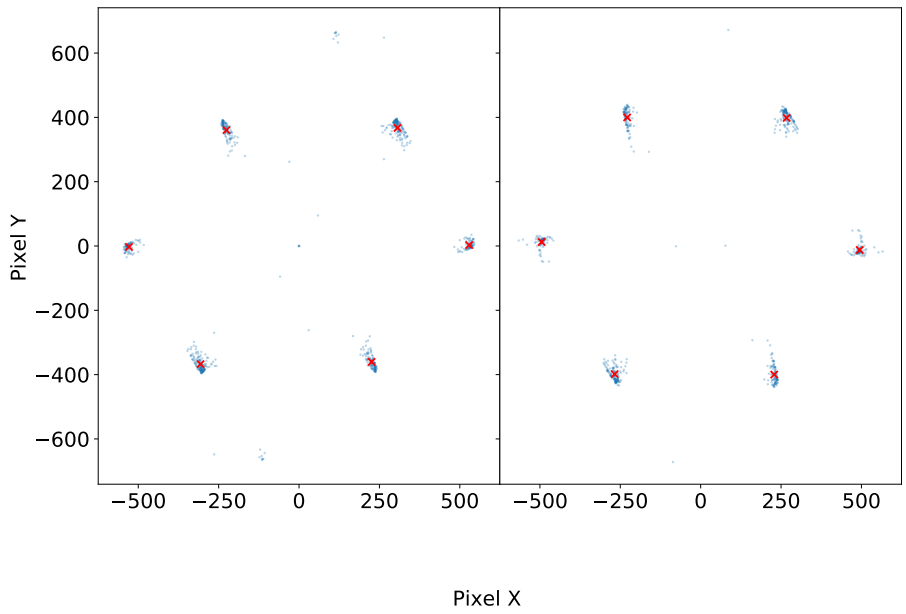


***Figure 4.2:*** *The difference vectors are plotted as blue dots and with the average difference vector for each cluster as red crosses. The red crosses represent the vertices of the deformed hexagon. The left plot uses the uncorrected images and the right plot the corrected images.*

### 4.1.1 First Metric: Variance in Clusters

Plotting the difference vectors for the corrected and uncorrected images results in figure 4.2. One can clearly see the clusters forming a hexagon. Taking the average vector in each cluster results in the red crosses seen in the figure. These will represent the deformed hexagon used for the metrics. There are some smaller clusters that can be seen which can be explained by occasional images that include an extra lattice point at the edge. These smaller clusters will not be taken into account.

The variance of each cluster from its respective average point is taken in two orthogonal dimensions and then divided by the number of points in the cluster. This results in two values per cluster. All twelve values are then summed up. The results can be seen in table 4.1.

### 4.1.2 Second and Third Metric: Variance in Distance From Origin and Variance in Angles

In the deformed hexagon the distance from each vertex to the origin is different. The variance in this set of 6 distances is the second metric.

As stated before, the angle between two vertices in a hexagon modulo 60, with the center as the reference point, is known to be 0 degrees. The third metric uses this as follows. Each angle between two of the cluster averages is taken modulo 60 degrees with the origin as reference point. Then, if the resulting angle is closer to 60 than to 0 degrees, its difference with 60 is taken. This is possible as it is expected for each angle in the deformed hexagon to be around 0 modulo 60 for both the uncorrected and corrected images. Given that the angle measured is $\theta$ the resulting angle $\theta'$ is given by:

$$\theta' = \mathbb{1}_{\{\theta \mod 60 \leq 30\}}(\theta \mod 60) + \mathbb{1}_{\{\theta \mod 60 > 30\}}(\theta \mod 60 - 60) \tag{4.1}$$

The variance of the resulting angles is the the third metric.

## 4.2 Subset Analysis

To derive the diffraction distortion $T$, the whole data set was used for the spline interpolation. However, one can derive the diffraction distortion with a subset of this data as well, resulting in different functions for the diffraction distortion. This might lead to a satisfactory correction that uses less data and thus is faster. In this section the metrics will be applied to the following 3 data sets. The uncorrected data, where the diffraction distortion is taken as the identity function. The corrected data which uses the whole data set and the corrected data using specific subsets of the data set. For the subsets $T$ will be approximated with spline interpolation using only the subset. However, the correction using the resulting approximation for $T$ will be applied to the entire data set.

The subsets are taken from the set represented by the coloured dots in figure 3.5 as this directly correlates to the set $B$ from figure 3.7. In the first subset every second row and column will be removed. Here 42 of the 182 points remain. For the second subset the goal is to take 25% from the center. This will be achieved by taking a circle in the center that includes a number of data points closest to 25% of the data. Here 44 of the 182 points remain. For the third data set the goal is to keep the 25% of the data points

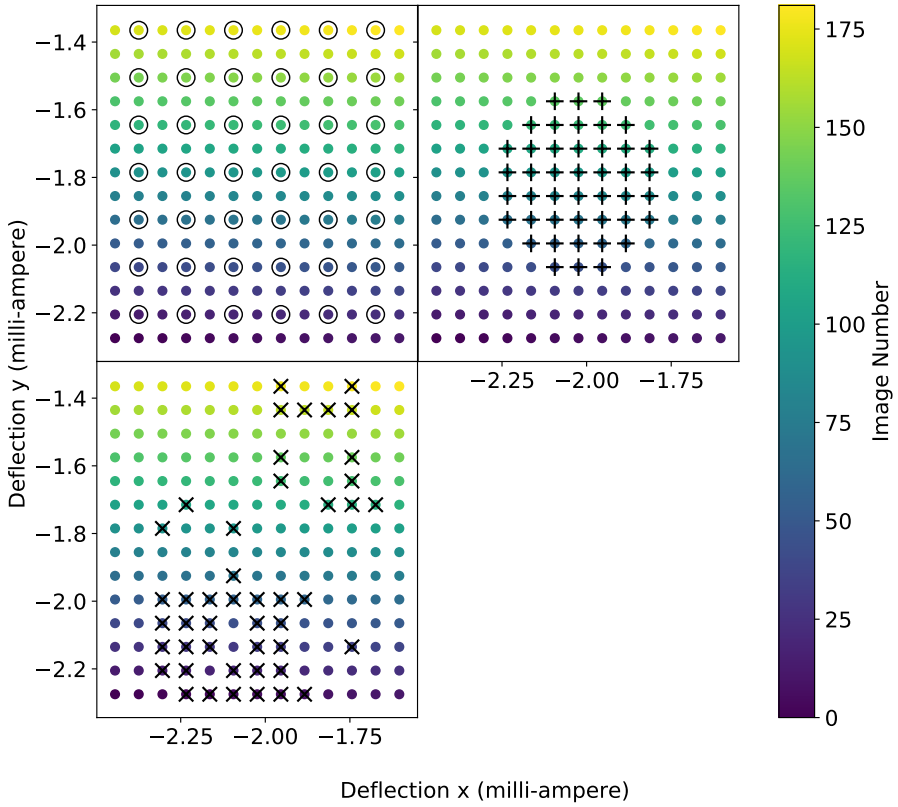


***Figure 4.3:*** *Each subplot shows figure 3.5 with a marked subset. Top left the first subset is marked with black circles. Top right the second subset is marked with black pluses. Bottom left the third subset is marked as black crosses.*

with the highest intensities. Again here the closest number of data points to 25% of the data is taken resulting in 46 of the 182 points remaining. The subset can be seen in figure 4.3.

The values obtained, rounded to 1 decimal point, are shown in table 4.1.

The variance in the clusters increases slightly from 30.3 pixels$^2$ to 41.9 pixels$^2$ when the correction is applied using the entire data set. Meanwhile the variance in distance decreases from 1761.8 pixels$^2$ to 195.8 pixels$^2$ and the variance in angles decreases from 64.1 degrees$^2$ to 5.5 degrees$^2$. Each subset of data increases the variance in clusters and decreases the variance in distances and angles. Most notably, when using the first subset instead



Version of August 12, 2022– Created August 12, 2022 - 09:51

***Table 4.1:*** *Results of Metrics*

| Data Set | Metric | | |
|---|---|---|---|
| | Variance in clusters (pixels$^2$) | variance in distance (pixels$^2$) | variance in angles (degrees$^2$) |
| Uncorrected | 30.3 | 1761.8 | 64.1 |
| Entire data set | 41.9 | 195.8 | 5.5 |
| Removing every second row and column | 40.2 | 388.3 | 13.7 |
| 25% from the center | 33.2 | 1259.0 | 45.9 |
| 25% of highest intensity data points | 34.3 | 403.8 | 15.0 |

of the entire data set the variance in the angles and distances double.

Chapter 5

# Discussion

In this section the success of the correction will be analysed using the metrics previously defined. We will also discuss the quality of the corrections based on the data subsets. Lastly the improvements that could be done in the method and the metrics will be discussed.

## 5.1 Success of the Correction

Looking at the results in table 4.1 the variance within each cluster increases from 30.3 pixels$^2$ when any correction is applied. However, from the second and third metric one can see that the variance in distance and angles decrease from 1761.8 pixels$^2$ and 64.1 angles$^2$ respectively. It becomes apparent that all of the corrections cause the average of the difference vectors to deviate less from the perfect hexagon. Using the entire data causes the biggest decrease. The variance of the average distance decreases by 1566 pixels$^2$ and the variance of the average angles by 58.6 angles$^2$ with the slight trade off in the variance in clusters increasing by 11.8 pixels$^2$. This trade off does become negligible when an average is taken over multiple data points. Because of this the correction is successful as it allows for accurate measurement of angles and distances.

## 5.2 Quality of Correction using Subsets

As expected, with less data the quality of the correction decreases. However, the type of subset does make a lot of difference. When looking at how well the subsets performed it becomes apparent that a wider range of data is much better than data that is close together in the center. This

can be seen by the fact that both the wider spread first and third subsets have variances of 388.3 pixels$^2$ and 403.8 pixels$^2$ respectively for the second metric and values of 13.7 angles$^2$ and 15 angles$^2$ respectively for the third metric. In comparison, the second subset, which was the least wide spread, has variances of 1259 pixels$^2$ and 45.9 angles$^2$ for the second and third metrics respectively. We conclude that if one wants to collect less data to save time, then taking a wider spread set is the way to go. The correction that the first subset provides is still lot better than the uncorrected data as the variances decrease by 1373.5 pixels$^2$ and 50.4 angles$^2$ in the second and third metrics respectively. Therefore, this subset still successfully allows for a better accuracy when measuring angles and distances. Also, one can investigate some more widespread subsets similar to the first subset as there is most probably one that provides a better correction than the first subset does.

We will now analyse how much worse the first subset is to using the entire data. As the purpose is for the measurement of angles and distances the focus will be on the last two metrics. The variance in distance increases by $(\frac{388.3}{195.8} - 1) \cdot 100 = 98.3\%$ and the variance in angles increases by $(\frac{13.7}{5.5} - 1) \cdot 100 = 149.1\%$ when using the first subset instead of the entire data. Using a fourth of the data thus approximately doubles the variance in distance and angles. When using the uncorrected data instead of the entire data the variance in distance increases by $(\frac{1761.8}{195.8} - 1) \cdot 100 = 799.8\%$ while the variance in angles increases by $(\frac{64.1}{5.5} - 1) \cdot 100 = 1065.5\%$. Because of this the trade-off from using the first subset instead of the entire data is very beneficial, and as stated before could be looked into more for even better results.

## 5.3 Restrictions and Improvements to Method and Metrics

The main improvement to the method would be a refinement to the detection of the nearest peak. As seen in figure 3.7, peaks are detected by looking for the highest intensity within a square of length 100 pixels around the expected position. For some peaks however, the peak is not fully inside this square, resulting in an error in the found peak position. This is a restriction in the method, but it does not play such a major role that it restricts us from drawing any good conclusions. This is because the current method is good enough so that only a few data points have a position that is slightly wrong.



Version of August 12, 2022– Created August 12, 2022 - 09:51

Another improvement is to more accurately measure the position of the peaks. Currently, as seen in figure 3.3, the maximum intensity is taken as the peak position. However, one can see that a peak is not a single position, instead it is spread over a small discrete area of high intensity. This discretization is caused by the detector. Using interpolation of the intensities one can make this cluster continuous and get a more accurate measurement of the position of the peak. This is a very minor improvement as it would only improve the approximation by maximum 0.5 pixels thus doesn't restrict our method very much.

The method of doing the intermediate steps for any of the metrics can be improved such that it better represents the quality of the correction. For all the metrics, the main improvement would be to the detection of the peaks in each image. Currently this is done by taking each peak that has an intensity above a certain threshold. However, unwanted peaks, usually from the edges of the images, occasionally fall above the threshold. The difference vectors caused by these are mostly easy to detect from figure 4.2 and can thus be removed. However, when one is located in one of the 6 main clusters it is not detected and therefore not removed. Another improvement would be to the algorithm used for detecting the clusters seen in figure 4.2. Currently, this is achieved by looking within a circle of a given radius around each difference vector in figure 4.2 and finding the clusters based off their unions. This is currently possible for the data as the clusters are very far from each other. However, some points are left out when the radius isn't chosen accurately or when a correction causes more widely spread clusters. Lastly, the angles taken for the third metric are not independent. This is a problem as it makes it more difficult to interpret the variance in relation to the data. However, the current metric is still an indicator for the deviation from a perfect hexagon which is what it is used for. Therefore the third metric is still a valid metric.

Chapter 6

# Conclusion

In this thesis we have developed a method for an in-place correction of the diffraction distortion present in a LEEM. By looking at a single Bragg peak and moving the sample in k-space a calibration image was formed from which the distortion can be calculated using spline interpolation. The calibration image shows the movement of this Bragg peak with the movement of the sample in k-space. This means a data set of multiple images is used to approximate the diffraction distortion.

The method presented in this thesis allows to accurately measure angles and distances, even when the distortion in the original data is so bad it is not possible at all. This is very clearly seen by the fact that measuring an angle in the uncorrected data has a variance of 64.1 degrees$^2$ while it only has a variance of 5.5 degrees$^2$ when corrected. The results suggest that if less of the data points are used, with a wide spread, the variance in both the distance and angles only increase slightly. With 25% of the data the variance in both the distance and angles doubles. However, with an even wider spread of data this could be achieved with even less data points and less of an increase in the variance. More research into this can thus be done. Other suggestions for future research include a better implementation of the nearest peak detection and cluster detection algorithms.

Chapter 7

# Appendix

## 7.1 Symbols used in Method

| | |
|---|---|
| $T$ | The transformation function that represents the diffraction distortion. |
| $B'$ | Pixel set that contains the distorted pixel positions of the Bragg peak as it moves in k-space. This pixel set is not a regular grid. |
| $B$ | Pixel set that contains the undistorted pixel positions of the Bragg peak as it moves in k-space. This pixel set is a regular grid. |
| $C$ | Deflector values for the movement of the sample in k-space. This pixel set is made to be a regular grid. |
| $L$ | The affine transformation from $C$ to $B$. |
| $M$ | Pixel set that contains the pixel positions of the highest intensity pixel in each image of the data set. |
| $C_{sub}$ | A subset of $C$ used for approximating the affine transformation $L$ |
| $B'_{sub}$ | A subset of $B'$ used for approximating the affine transformation $L$ |
| $A$ | 2-by-2 matrix that represents the linear part of the affine transformation $L$ |

# Bibliography


[1] F. Sojka, M. Meissner, C. Zwick, R. Forker, and T. Fritz, *Determination and correction of distortions and systematic errors in low-energy electron diffraction*, Review of Scientific Instruments **84**, 015111 (2013).

[2] S. H. Simon, *The Oxford Solid State Basics.*, OUP Oxford, 2013.

[3] J. Kautz, *Low-energy electron microscopy on two-dimensional systems:: growth, potentiometry and band structure mapping*, PhD thesis, Leiden Institute of Physics (LION), Faculty of Science, Leiden Univesity, 2015.

[4] R. Tromp, J. Hannon, W. Wan, A. Berghaus, and O. Schaff, *A new aberration-corrected, energy-filtered LEEM/PEEM instrument II. Operation and results*, Ultramicroscopy **127**, 25 (2013), Frontiers of Electron Microscopy in Materials Science.

[5] P. Thévenaz, T. Blu, and M. Unser, *Image interpolation and resampling*, Handbook of medical imaging, processing and analysis **1**, 393 (2000).

[6] A. Jeffrey, *Advanced Engineering Mathematics.*, Academic Press, 2002.